Electronic structures and *p-d* exchange interaction of Mn-doped diluted magnetic semiconductors

S. Ueda,[1,*] A. Sekiyama,[2] T. Iwasaki,[2] S. Imada,[3] S. Suga,[2] Y. Saitoh,[4] W. Giriat,[5] and S. Takeyama[6]
[1]*NIMS Beamline Station at SPring-8, National Institute for Materials Science, Sayo, Hyogo 679-5148, Japan*
[2]*Department of Materials Physics, Graduate School of Engineering Science, Osaka University, Toyonaka, Osaka 560-8531, Japan*
[3]*Department of Physical Science, College of Science and Engineering, Ritsumeikan University, Kusatsu, Shiga 525-8577, Japan*
[4]*Synchrotron Radiation Research Center, Japan Atomic Energy Agency, Sayo, Hyogo 679-5148, Japan*
[5]*Centro de Fisica, Instituto Venezolano de Investigaciones Cientificas, Caracas 1020A, Venezuela*
[6]*The Institute for Solid State Physics, The University of Tokyo, Kashiwa, Chiba 277-8581, Japan*
(Received 30 July 2008; published 25 November 2008)

Electronic structures of Mn-doped II-VI diluted magnetic semiconductors (DMSs) were studied by Mn $2p$ core absorption (XAS), Mn $2p$ core-level photoelectron (XPS), and Mn $2p$-$3d$ resonance photoelectron spectroscopy (RPES). The Mn $2p$ XAS, $2p$ XPS, and $2p$-$3d$ RPES spectra were analyzed by configuration-interaction theory based on the cluster model. We then obtained a strong negative p-d exchange constant between anion p bands and Mn $3d$ orbitals for the wide gap DMSs $Zn_{1-x}Mn_xSe$ and $Zn_{1-x}Mn_xS$. In contrast, for the narrow gap DMS $Hg_{1-x-y}Cd_xMn_yTe$, we found a weak negative p-d exchange constant. By comparing these results with the results of the previous work, we found that the p-d exchange constant in wide and narrow gap II-VI DMSs is proportional to the absolute band-gap energy. This phenomenon can be interpreted by the change in the density of states of anion p bands, which hybridized with the Mn $3d$ orbitals, at the valence-band maximum. These results suggest that one can control the p-d exchange interaction in DMSs by changing the band-gap energy.

DOI: 10.1103/PhysRevB.78.205206 PACS number(s): 75.50.Pp, 81.05.Dz, 79.60.−i

I. INTRODUCTION

It is well known that diluted magnetic semiconductors (DMSs) have both the semiconducting and magnetic properties. Especially Mn-doped II-VI DMSs have attracted considerable interest due to their characteristic optical, magnetic, and transport properties such as tunable band-gap energy by the Mn substitution, giant Zeeman splitting, negative magnetoresistance, and so on.[1,2] It is experimentally and theoretically indicated that the sp-d exchange interaction between host sp bands and localized $3d$ orbitals of transition metal plays an important role for the physical properties. To understand the physical properties of DMSs, the electronic structures of $Cd_{1-x}Mn_xY$ (Refs. 3 and 4) and $Zn_{1-x}Mn_xY$ (Y=S,Se,Te) (Refs. 5 and 6) were studied by photoelectron spectroscopy (PES). The Mn $3d$ partial electronic structures for $Cd_{1-x}Mn_xY$ (Y=S,Se,Te), which were obtained by the Mn $3p$-$3d$ resonance PES (RPES), were understood by configuration-interaction (CI) theory based on Mn Y_4 cluster model.[3,7] The importance of the p-d hybridization between the anion p bands and localized Mn $3d$ orbitals was shown in the theoretical calculation. The evaluated p-d exchange constant ($N\beta$) from the CI cluster model calculation[7,8] was consistent with $N\beta$ obtained by the magnet-optic measurement.[1,2] It is known that the p-d exchange interaction through the p-d hybridization is stronger in magnitude than the s-d exchange interaction derived from the direct exchange. Thus the p-d exchange interaction is an important physical quantity to understand the physical properties of DMSs.

$Cd_{1-x}Mn_xY$ and $Zn_{1-x}Mn_xY$ (Y=S,Se,Te) belong to wide gap II-VI DMSs. As mentioned above, many experiments have been performed to understand the electronic structures of $Cd_{1-x}Mn_xY$ and $Zn_{1-x}Mn_xY$ (Y=S,Se,Te) by means of PES. In contrast few experiments for narrow gap II-VI DMSs using PES were reported.[9] As seen in Refs. 2 and 10, the p-d exchange constant seems to depend on the band-gap energy of host semiconductors. However there is no study about how the p-d exchange interaction depends on the band-gap energy of host semiconductors, while there are many studies about how magnetic and optical properties depend on the concentration of magnetic impurity in semiconductors.[1,2]

In this paper, we investigate the electronic structures and p-d exchange interaction of wide and narrow gap DMSs $Zn_{1-x}Mn_xY$ (Y=S,Se) and $Hg_{1-x-y}Cd_xMn_yTe$ by using Mn $2p$ core PES (XPS), Mn $2p$ core absorption spectroscopy (XAS), Mn $2p$-$3d$ RPES, and the CI cluster model calculation. A rich variety of bulk samples in the Mn-doped II-VI DMSs is suitable for the study of the band-gap dependence on the p-d exchange interaction. Core-level XPS and XAS are element-specific measurements and display the electronic states such as hybridized states and valency. The resonance enhancement of photoelectron intensity in the $2p$-$3d$ excitation region of $3d$ transition metals is much more prominent than that in the $3p$-$3d$ excitation region. RPES in the $2p$-$3d$ excitation region is very useful for detecting the $3d$ electronic structures even though a $3d$ transition-metal concentration is nearly 1 at % as seen in our previous work for $Hg_{1-x-y}Cd_xMn_yTe$.[9] Combining two element-specific measurements of XAS and PES, we can obtain the reliable electronic structure parameters from the CI cluster model calculation. Detailed analysis of the electronic structures and p-d exchange interaction of $Zn_{1-x}Mn_xY$ (Y=S,Se) and $Hg_{1-x-y}Cd_xMn_yTe$ has been done to discuss the band-gap energy dependence in this work by comparing the present result with the results of the traditional DMS $Cd_{1-x}Mn_xTe$.

We believe that the systematic analysis of the *p-d* exchange interaction in II-VI DMSs gives us helpful information to clarify the ferromagnetism in DMSs,[11–14] because the *p-d* exchange interaction is considered as one of the important interactions for the origin of the ferromagnetism in the DMSs.

II. EXPERIMENT

The single crystalline $Zn_{1-x}Mn_xY$ (Y=Se,S) was prepared by Bridgeman method. The detail for the sample preparation was described in Ref. 15. The manganese compositions and the crystal structures of $Zn_{1-x}Mn_xY$ were determined by x-ray powder diffraction. $Zn_{1-x}Mn_x$Se and $Zn_{1-x}Mn_x$S had the zinc-blende structure with x=0.098 and wurtzite structure with x=0.177, respectively. For Mn 2*p* XPS, an x-ray tube (Mg $K\alpha$: $h\nu$=1253.6 eV) was used as an excitation photon source. The Mn 2*p* XPS spectra were measured by a double-pass cylindrical mirror analyzer. Mg $K\alpha$ satellite lines were numerically subtracted from the XPS spectra. Clean sample surfaces were obtained by scraping *in situ* with a diamond file in an ultrahigh vacuum (UHV) chamber with the base pressure of 4.5×10^{-8} Pa. Total-energy resolution was set to about 1 eV. The sample was cooled by liquid nitrogen and the sample temperature was about 130 K. The Mn 2*p* XAS was performed at the soft x-ray undulator beamline BL25SU (Refs. 16 and 17) of SPring-8. Clean sample surfaces were obtained by scraping *in situ* with a diamond file in UHV at the base pressure of 7.2×10^{-8} Pa. The energy resolution of XAS was set to about 0.2 eV in the Mn 2*p*-3*d* excitation region. XAS measurements were performed by the total photoelectron yield method at room temperature. The samples were illuminated by a standard halogen lump to prevent the electrostatic charging effect during XPS and XAS measurements.

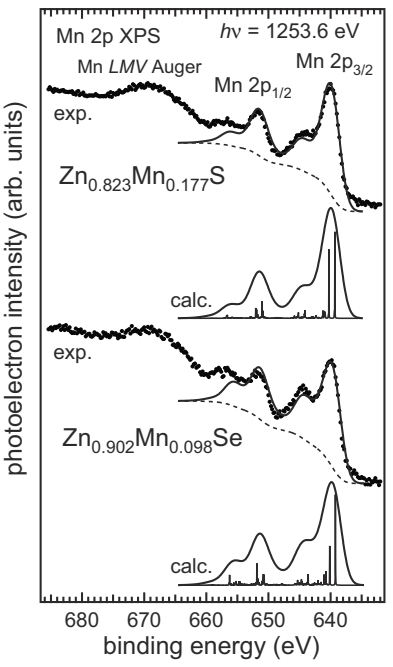

FIG. 1. Experimental (dots) and calculated (solid curves) Mn 2*p* XPS spectra of $Zn_{1-x}Mn_xY$ (Y=S,Se). The parameters for CI cluster model calculation are listed in Table I.

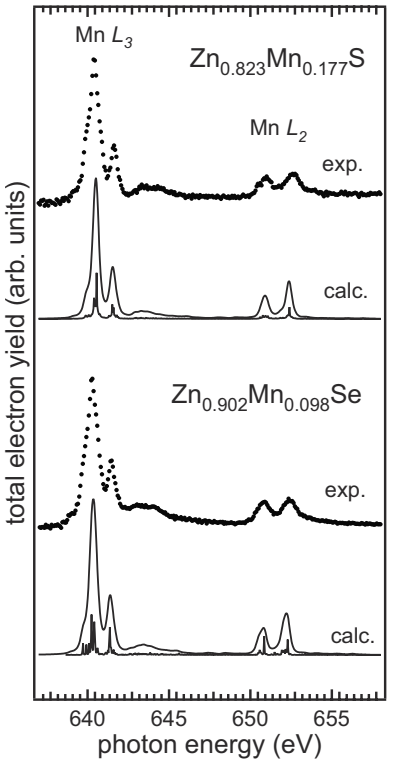

FIG. 2. Experimental (dots) and calculated (solid curves) Mn 2*p* XAS spectra of $Zn_{1-x}Mn_xY$ (Y=S,Se). The calculated Mn 2*p* XAS spectra are obtained by using the same parameter set as in the Mn 2*p* XPS calculations listed in Table I.

The single crystalline highly homogeneous $Hg_{1-x-y}Cd_xMn_y$Te was prepared by modified two-phase mixture crystal-growth method.[18] The sample with the zinc-blende structure was taken from the ingot, whose composition was evaluated by mass-density measurement and x-ray microprobe analysis.[18] RPES and XAS measurements were performed at the soft x-ray undulator beamline BL25SU (Refs. 16 and 17) of SPring-8 using the high-resolution electron spectrometer of SCIENTA SES200 analyzer. Clean sample surfaces of $Hg_{1-x-y}Cd_xMn_y$Te were obtained by cleavage in UHV at the base pressure of 5.0×10^{-8} Pa. The energy resolutions of both RPES and XAS were set to about 0.2 eV in the Mn 2*p*-3*d* excitation region. XAS measurements were performed by the total photoelectron yield method. The cleanliness of the sample surfaces was checked by the weakness of O 1*s* and C 1*s* peaks before and after each measurement at 20 K. We note that the samples in the paramagnetic state were measured in these experiments.

III. RESULTS AND DISCUSSION

A. Mn 2*p* XPS and XAS for $Zn_{1-x}Mn_xY$ (Y=Se,S)

Figure 1 shows the experimental Mn 2*p* XPS spectra (dots) for $Zn_{1-x}Mn_xY$ (Y=Se and S). In these spectra, the spin-orbit doublet (Mn $2p_{3/2}$ and Mn $2p_{1/2}$) and remarkable satellite structures on the higher-binding-energy side of the

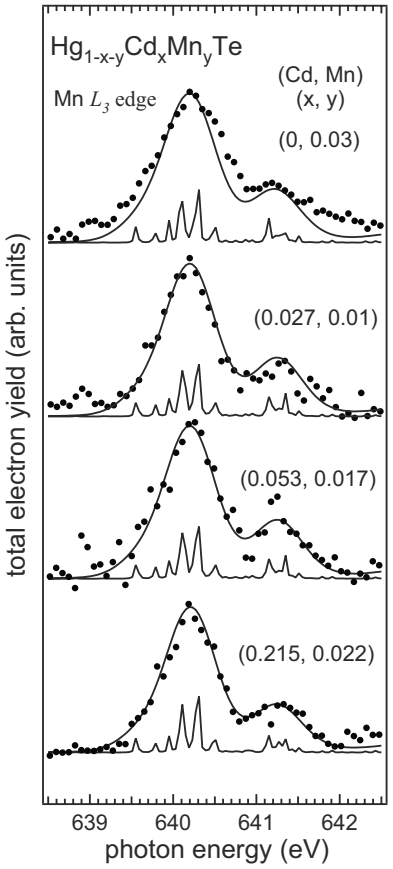

FIG. 3. Experimental (dots) and calculated (solid curves) Mn $2p$ XAS spectra of $Hg_{1-x-y}Cd_xMn_yTe$ with $x=0-0.215$ and $y\sim0.02$ around the Mn L_3 absorption edge (Ref. 9). The parameters for the CI cluster model calculation are listed in Table I.

main peaks were observed. Relative intensity of the satellite to the main peak for $Y=$Se was found to be stronger than that for $Y=$S. The broad structure around 670 eV is due to the Mn LMV ($2p3p3d$) Auger emission. The presence of the satellite structures indicates that the Mn $3d$ electronic state is influenced not only by strong Coulomb interaction between Mn $3d$ electrons but also by the hybridization between the Mn $3d$ orbitals and anion p bands.

Figure 2 shows the Mn $2p$ XAS spectra (dots) for $Zn_{1-x}Mn_xY$ ($Y=$Se, S). These spectra were normalized at the main absorption peak (640.3 eV) after subtraction of a linear background. The Mn $2p$ XAS spectra for $Y=$S and Se are roughly classified into two parts due to the spin-orbit splitting of the Mn $2p$ core level. The L_3 and L_2 absorptions are located at 638–646 and 649–655 eV, respectively. The observed spectra were similar to the previously reported Mn $2p$ XAS spectrum for $Zn_{0.90}Mn_{0.10}S$.[19] By comparing these spectra with the theoretical calculation of the Mn $2p$ XAS spectra for tetragonal symmetry,[20] we see that the complicated multiplet structures of the Mn $2p$ XAS spectra for $Y=$S and Se are mainly due to the $2p^53d^6$ final states after the dipole transition. In addition the crystal-field splitting 10 Dq is found to be negligible. Taking the results of the Mn $2p$ XPS and XAS for $Zn_{1-x}Mn_xY$ ($Y=$Se and S) into account, we conclude that the Mn ions are dominantly divalent while

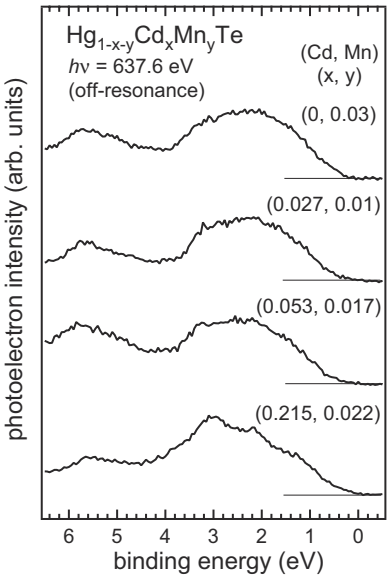

FIG. 4. Valence-band PES spectra of $Hg_{1-x-y}Cd_xMn_yTe$ with $x=0-0.215$ and $y\sim0.02$ taken at $h\nu=637.9$ eV. This excitation photon energy is lower than the Mn $2p$ core absorption energy.

the hybridization between the Mn $3d$ orbitals and anion p bands is important for $Zn_{1-x}Mn_xY$.

B. Mn $2p$ XAS and $2p$-$3d$ RPES for $Hg_{1-x-y}Cd_xMn_yTe$

Figure 3 shows the experimental Mn $2p$ XAS spectra (dots) for $Hg_{1-x-y}Cd_xMn_yTe$ with $x=0-0.215$ and $y\sim0.02$ in the Mn L_3 absorption region.[9] The Mn L_3 main absorption peak and the satellite structure are located at 640.2 and 641.5 eV, respectively. These spectra were normalized by the intensity at the Mn L_3 absorption peak after subtraction of a linear background. The spectral structures of the Mn $2p$ XAS were similar with each other, but the relative intensity between the main peak and satellite structure was found to be slightly different for the various Cd compositions (x). The intensity of the satellite structure slowly decreased with increasing Cd x. The experimental Mn $2p$ XAS spectra are similar to the theoretical Mn $2p$ XAS spectrum for the $2p^53d^6$ final states.[20]

The valence-band PES spectra (solid curves) for $Hg_{1-x-y}Cd_xMn_yTe$ with $x=0-0.215$ and $y\sim0.02$ are shown in Fig. 4. The excitation photon energy was set at 637.6 eV. This energy is lower than the Mn $2p$ core absorption energy as seen in Fig. 3. We note that the binding energy was referred to the Fermi level of an evaporated Au film. It was observed that the valence-band structure is modified by the change in Cd x. The intensity of the structure at 3 eV increased with increasing Cd x. The binding energy of the hump around 5.5 eV decreased with increasing Cd x. These modifications in the valence-band structure of $Hg_{1-x-y}Cd_xMn_yTe$ are interpreted by the change in the electronic structure due to the negative to positive band-gap transition as seen in the previous PES and theoretical studies of $Hg_{1-x}Cd_xTe$.[21,22]

Figure 5 shows the valence-band PES spectra of $Hg_{0.97}Mn_{0.03}Te$ in the Mn $2p$-$3d$ excitation region. Inset of

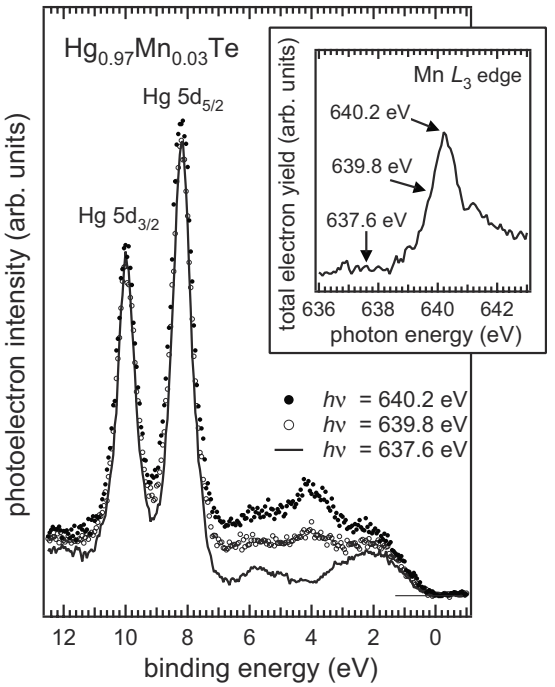

FIG. 5. Enhancement of photoelectron intensity in the valence-band region for $Hg_{0.97}Mn_{0.03}Te$ measured with the excitation photon energy around the Mn L_3 absorption edge. Off-resonance (solid curve), resonance (open circles), and resonance maximum (closed circles). Inset shows the Mn $2p$ XAS spectrum for $Hg_{0.97}Mn_{0.03}Te$ around the Mn L_3 absorption edge.

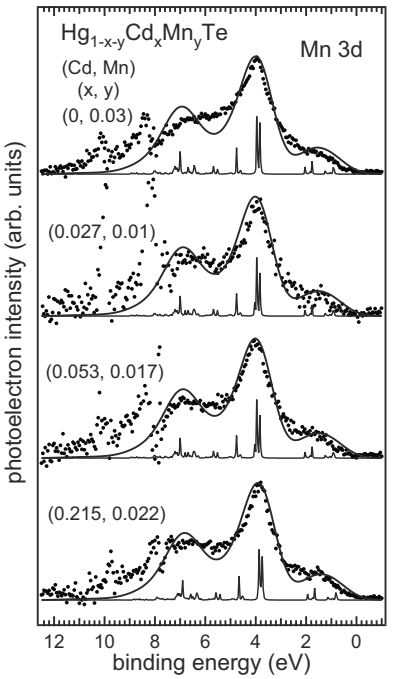

FIG. 6. Experimental Mn $3d$ PES spectra (dots) for $Hg_{1-x-y}Cd_xMn_yTe$ with $x=0-0.215$ and $y\sim0.02$ obtained by subtraction of off-resonance spectra from on-resonance one (Ref. 9). The calculated Mn $3d$ PES spectra (solid curves) are obtained by using the same parameter set for the Mn $2p$ XAS calculations listed in Table I.

Fig. 5 shows the Mn $2p$ XAS spectrum of $Hg_{0.97}Mn_{0.03}Te$. The off-resonance spectra (solid curve) taken at $h\nu=637.6$ eV shows that the Te $5p$ bands are located between 0 and 7 eV and the spin-orbit doublet of Hg $5d_{5/2}$ and Hg $5d_{3/2}$ peaks are located at 8 and 10 eV, respectively. In the Mn $2p$-$3d$ on-resonance excitation, enhancement of photoelectron intensity was clearly observed around 4 eV for both spectra taken at $h\nu=639.8$ (open circles) and 640.2 eV (closed circles). This enhancement is due not to simple Auger electrons but to the direct recombination process. Therefore the enhanced spectral weight reflects the Mn $3d$ derived feature. The Mn $3d$ partial electronic structures for $Hg_{1-x-y}Cd_xMn_yTe$ with $x=0-0.215$ and $y\sim0.02$ were obtained by subtracting the off-resonance spectrum taken at $h\nu=637.6$ eV from the on-resonance spectrum taken at 640.2 eV.

Figure 6 shows the experimentally obtained Mn $3d$ PES spectra (dots) of $Hg_{1-x-y}Cd_xMn_yTe$ with $x=0-0.215$ and $y\sim0.02$.[9] These spectra were normalized at the main peak intensity at 4 eV. The Mn $3d$ PES spectra show a hump, a main peak, and a broad satellite structure near 1, 4, and 7 eV, respectively. Similar spectral features were observed in traditional DMS $Cd_{1-x}Mn_xTe$ in the Mn $3p$-$3d$ excitation region.[3] The structures in the region between 8 and 10 eV are artificial due to the failure of subtraction of the relatively strong Hg $5d_{5/2}$ and Hg $5d_{3/2}$ peaks in the off-resonance spectra. The Mn $3d$ spectra were similar each other, but the relative intensity between the main peak and satellite (hump) structure was found to be slightly different for the various Cd x. For $Hg_{1-x-y}Cd_xMn_yTe$ with $x(Cd)=0$ and $y(Mn)=0.03$, the intensity of the satellite structure between 5 and 7 eV sloped down to the higher-binding-energy side. In contrast, the intensity of the satellite structure sloped up for $Hg_{1-x-y}Cd_xMn_yTe$ with $x(Cd)=0.215$ and $y(Mn)=0.022$. It was reported in the CI cluster model calculation for $Cd_{1-x}Mn_xTe$ that the relative intensities of the satellite and hump structures to the main peak were modified by the change in the strength of the p-d hybridization between the Mn $3d$ orbitals and anion p bands.[3] Thus it is expected that the p-d hybridization in $Hg_{1-x-y}Cd_xMn_yTe$ is modified by the change in the host valence-band structure due to the Cd doping.

C. Cluster model analysis of XAS, XPS, and RPES spectra for Mn-doped DMSs

In order to quantitatively interpret the Mn $2p$ XAS, XPS, and Mn $3d$ PES spectra, we have carried out the CI cluster model calculation considering the $|3d^5\rangle$, $|3d^6\underline{L}\rangle$, and $|3d^7\underline{L}^2\rangle$ states in the Mn ground state, where $\underline{L}$ denotes a hole in the ligand p bands. In the calculation the p bands are replaced with two discrete energy levels, which are separated by 1 eV, to roughly treat the valence-band structure. The employed parameters for the CI cluster model calculation are as follows. The charge-transfer energy is defined as $\Delta=E(3d^6\underline{L})-E(3d^5)$. Each term is the center of gravity of the multiplet states of the corresponding configuration. The p-d transfer integrals of $(pd\sigma)$ and $(pd\pi)$ with the relation $(pd\sigma)/(pd\pi)=-2.17$ (Ref. 23) are used in the calculation. The $3d$-$3d$ and $3d$-$2p$ Coulomb interactions are denoted by

TABLE I. Electronic structure parameters for $Zn_{1-x}Mn_xY$ (Y=S,Se) and $Hg_{1-x-y}Cd_xMn_yTe$ with x =0–0.215 and $y\sim0.02$. Δ, $(pd\sigma)$, and U_{dd} are given in units of eV. n_d is the number of $3d$ electron.

		Δ	$(pd\sigma)$	U_{dd}	n_d
$Zn_{1-x}Mn_xS$	x=0.177	3.0	1.08	4.0	5.17
$Zn_{1-x}Mn_xSe$	x=0.098	2.5	1.04	4.0	5.17
$Hg_{1-x-y}Cd_xMn_yTe$	x=0, y=0.03	2.0	0.85	4.0	5.15
$Hg_{1-x-y}Cd_xMn_yTe$	x=0.027, y=0.01	2.0	0.73	4.0	5.15
$Hg_{1-x-y}Cd_xMn_yTe$	x=0.053, y=0.017	2.0	0.73	4.0	5.15
$Hg_{1-x-y}Cd_xMn_yTe$	x=0.215, y=0.022	2.0	0.79	4.0	5.15

$U_{dd}=E(3d^{n+1})+E(3d^{n-1})-2E(3d^n)$ and $U_{dc}=[E(3d^{n+1})-E(3d^n)]-[E(3d^{n+1}\underline{c})-E(3d^n\underline{c})]$, respectively, where $\underline{c}$ denotes a hole in the Mn $2p$ core level. Here, the relation $U_{dd}/U_{dc}=0.8$ is assumed.[24] The Slater integrals are obtained by reducing the Hartree-Fock values by the factor of 0.8.[20] We note that the effect of the resonance process to the spectral shape is ignored in the Mn $3d$ PES calculation for simplicity.

The calculated Mn $2p$ XPS spectra (solid curves) for $Zn_{1-x}Mn_xY$ (Y=Se and S) are shown in Fig. 1. The calculated spectra were broadened with a Gaussian (total-energy resolution) and a Lorentzian ($\sim$0.2 eV). Assuming the integrated background (broken curves), the calculation reproduces the experimental results of Mn $2p$ XPS for $Zn_{1-x}Mn_xY$ (Y=Se and S). The optimized parameters set for the calculation is listed in Table I. In the calculation, the crystal-field splitting 10 Dq is neglected according to the discussion above. The deviations at the satellite structures for the $2p_{1/2}$ peak are due to the energy-loss structures of the $2p_{3/2}$ peak. Taking the parameters set for the calculation into account, we found that the dominant component of satellite (main) structure corresponds to the $|2p^53d^5\rangle$ ($|2p^53d^6\underline{L}\rangle$) final states for each material. The weights of the configurations $3d^5$, $3d^6\underline{L}$, and $3d^7\underline{L}^2$ in the Mn ground state for $Zn_{1-x}Mn_xS$ ($Zn_{1-x}Mn_xSe$) are 84.2 (83.5)%, 15.1 (15.8)%, and 0.7 (0.7)%, respectively. The number of $3d$ electron is 5.17 for each material. The ratio of $|3d^6\underline{L}\rangle$ to $|3d^5\rangle$ in the ground state for $Zn_{1-x}Mn_xSe$ is slightly larger than that for $Zn_{1-x}Mn_xS$. This is caused by the difference of Δ, which gives the different intensity ratio of the satellite to main peak in Mn $2p$ XPS spectra. By using the parameter sets obtained from the Mn $2p$ XPS calculation, the basic features of the experimental Mn $2p$ XAS spectra for $Zn_{1-x}Mn_xY$ (Y=S and Se) are also reproduced by the calculated spectra (solid curves) as seen in Fig. 2. Thus the obtained electronic structure parameters for $Zn_{1-x}Mn_xY$ (Y=S,Se) is considered to be reliable, because the experimental Mn $2p$ XPS and XAS spectra are consistently reproduced by the calculations using the same parameters listed in Table I. These parameters for $Zn_{1-x}Mn_xY$ (Y=S,Se) agree with those reported in the theoretical work by Mizokawa and Fujimori.[7]

The calculated Mn $2p$ XAS and $3d$ PES spectra (solid curves) for $Hg_{1-x-y}Cd_xMn_yTe$ (Ref. 9) are shown in Figs. 3 and 6, respectively. The employed parameter sets for the calculation are listed in Table I. The crystal-field splitting of 10 Dq is also negligible for $Hg_{1-x-y}Cd_xMn_yTe$. The experimental Mn $2p$ XAS and $3d$ PES spectra for $Hg_{1-x-y}Cd_xMn_yTe$ are consistently reproduced by the calculation using the single parameter set for each set of (x,y). Thus we obtained the reliable electronic structure parameters for $Hg_{1-x-y}Cd_xMn_yTe$. The weights of the configurations $3d^5$, $3d^6\underline{L}$, and $3d^7\underline{L}^2$ in the Mn ground state for $Hg_{1-x-y}Cd_xMn_yTe$ are 85.6%, 13.9%, and 0.5%, respectively. The number of $3d$ electron is found to be 5.15 for $Hg_{1-x-y}Cd_xMn_yTe$. One can see that the slight difference in the experimental Mn $2p$ XAS and $3d$ PES spectra among the different sets of (x,y) is represented by the narrow spread of the p-d transfer integral $(pd\sigma)$ as seen in Table I. The parameters Δ and U_{dd} for $Hg_{1-x-y}Cd_xMn_yTe$ are comparable to the typical DMS $Cd_{1-x}Mn_xTe$, but $(pd\sigma)$ for $Hg_{1-x-y}Cd_xMn_yTe$ is smaller than that for $Cd_{1-x}Mn_xTe$.[7] This result implies that $(pd\sigma)$ becomes larger with increasing the band-gap energy in II-VI DMSs.

The number of $3d$ electron is found to be almost same for $Zn_{1-x}Mn_xY$ (Y=S,Se) and $Hg_{1-x-y}Cd_xMn_yTe$. As seen in Table I, both of the p-d transfer integral $(pd\sigma)$ and the charge-transfer energy Δ for $Zn_{1-x}Mn_xY$ (Y=S,Se) is larger than that for $Hg_{1-x-y}Cd_xMn_yTe$. Due to the larger $(pd\sigma)$ for $Zn_{1-x}Mn_xY$ (Y=S,Se) compared with $Hg_{1-x-y}Cd_xMn_yTe$, the weights of the configurations $3d^5$, $3d^6\underline{L}$, and $3d^7\underline{L}^2$ in the Mn ground state are almost the same in each sample, whereas Δ for $Zn_{1-x}Mn_xY$ (Y=S,Se) is larger than that for $Hg_{1-x-y}Cd_xMn_yTe$.

D. *p-d* exchange interaction in DMSs

By using the above-mentioned electronic structure parameters, we have evaluated the p-d exchange constant $N\beta$ for $Zn_{1-x}Mn_xY$ and $Hg_{1-x-y}Cd_xMn_yTe$. The p-d exchange constant $N\beta$ reflects the p-d exchange interaction through a hybridization between the Mn $3d$ orbitals and anion p bands. $N\beta$ is given by the second-order perturbation[2,7,8] as follows:

$$N\beta \approx -\frac{16}{S}V_{pd}^2\left(\frac{1}{U_{\text{eff}}-\delta_{\text{eff}}}+\frac{1}{\delta_{\text{eff}}}\right), \tag{1}$$

$$V_{pd}=\frac{1}{3}(pd\sigma)-\frac{2\sqrt{3}}{9}(pd\pi), \tag{2}$$

where δ_{eff} and U_{eff} are the same as Δ and U_{dd} defined in Sec. III C except that the state with the lowest energy is chosen for each configuration in the definition of δ_{eff} and U_{eff}. V_{pd} is the strength of p-d hybridization between the anion p and Mn $3d$ orbitals. The magnitude of local spin S=5/2 is assumed in the evaluation.

TABLE II. Band-gap energy and the *p-d* exchange constant $N\beta$ for $Zn_{1-x}Mn_xY$ (Y=S,Se) and $Hg_{1-x-y}Cd_xMn_yTe$ with x=0–0.215 and $y\sim0.02$. The band-gap energy and *p-d* exchange constant $N\beta$ are given in units of eV.

		Band-gap energy	$N\beta$
$Zn_{1-x}Mn_xS$	x=0.177	~3.8 [a]	−1.15 [b]
$Zn_{1-x}Mn_xSe$	x=0.098	~2.8 [a]	−1.07 [b]
$Hg_{1-x-y}Cd_xMn_yTe$	x=0, y=0.03	−0.200 [c]	−0.62 [b]
$Hg_{1-x-y}Cd_xMn_yTe$	x=0.027, y=0.01	−0.173 [c]	−0.44 [b]
$Hg_{1-x-y}Cd_xMn_yTe$	x=0.053, y=0.017	−0.146 [c]	−0.44 [b]
$Hg_{1-x-y}Cd_xMn_yTe$	x=0.215, y=0.022	0.181[c]	−0.50 [b]
$Cd_{1-x}Mn_xTe$	x=0.005	~1.6 [a]	−0.88 [d]

[a]Reference 2.
[b]This work.
[c]Reference 18.
[d]Reference 21.

The *p-d* exchange constant $N\beta$ and band-gap energy for $Zn_{1-x}Mn_xY$ (Y=S,Se) and $Hg_{1-x-y}Cd_xMn_yTe$ with x=0–0.215 and $y\sim0.02$ are listed in Table II. The evaluated $N\beta$'s for $Zn_{1-x}Mn_xY$ (Y=S,Se) are stronger in magnitude than that for traditional DMS $Cd_{1-x}Mn_xTe$, while those for $Hg_{1-x-y}Cd_xMn_yTe$ are weaker in magnitude than that for $Cd_{1-x}Mn_xTe$. The evaluated $N\beta$'s for $Zn_{1-x}Mn_xS$ and $Zn_{1-x}Mn_xSe$ are −1.15 and −1.07 eV, respectively. These values are consistent with the previous theoretical work for $Zn_{1-x}Mn_xY$ (Y=S,Se).[7] For $Hg_{1-x-y}Cd_xMn_yTe$ with x=0–0.215 and $y\sim0.02$, the obtained $N\beta$ is varied from −0.44 to −0.62 eV in our calculation. These values are rather consistent with −0.73 eV for $Hg_{1-x-y}Cd_xMn_yTe$ (Ref. 25) and −0.6 eV for $Hg_{1-x}Mn_xTe$ (Ref. 26) reported in the previous works. For $Cd_{1-x}Mn_xTe$, $N\beta$=−0.88 eV was reported.[27] One sees that the *p-d* exchange constant for the wide gap DMSs is stronger in magnitude than that for narrow gap DMSs. This tendency is also seen in Ref. 2.

In order to clarify a variety of the *p-d* exchange constants in II-VI group DMSs, we first consider the electronic structure parameters for $Hg_{1-x-y}Cd_xMn_yTe$ in comparison with those for traditional DMS $Cd_{1-x}Mn_xTe$. We note that only one parameter, $(pd\sigma)$, is different between $Hg_{1-x-y}Cd_xMn_yTe$ and $Cd_{1-x}Mn_xTe$.[7] It might seem that the difference in $(pd\sigma)$ is related to the Mn-Te bond length, because the strength of $(pd\sigma)$ increases as the bond length decreases.[23] However, the difference in the mean lattice constant between $Cd_{1-x}Mn_xTe$ and $Hg_{1-x}Mn_xTe$ is quite small when the Mn concentration is the same in each material.[28] In addition it was reported in the extended x-ray absorption fine-structure (EXAFS) study[29–31] that the Mn-anion bond length is independent on the Mn concentration in the II-VI group DMSs even though the mean lattice constant obeys Vegard's law.[28] Thus the variety of $(pd\sigma)$ in $Hg_{1-x-y}Cd_xMn_yTe$ and $Cd_{1-x}Mn_xTe$ cannot be explained by the difference of the mean lattice constant and Mn-Te bond length.

Next we consider whether the *p-d* exchange constant $N\beta$ is related to the band-gap energy or not. The band-gap energies for $Hg_{1-x-y}Cd_xMn_yTe$ and $Cd_{1-x}Mn_xTe$ are separated, while the electronic structure parameters excluding $(pd\sigma)$ are not different between them. We could not find a simple relation between the band-gap energy and *p-d* exchange constant $N\beta$ shown in Table II but found that the *p-d* exchange constant $N\beta$ increases with the absolute band-gap energy increasing as seen in Fig. 7(a). In addition, for other II-VI DMSs, the relation between the *p-d* exchange constant $N\beta$ (Refs. 2, 7, 8, and 32) and the absolute value of the band-gap energy[2] is found to be proportional as seen in Fig. 7(b). In the figure the band-gap energy at liquid He temperature for the Mn concentration nearly zero is used for comparison. From the least-squares fitting, we obtain the relation $N\beta$=−0.23$|E_g|$−0.56, where $|E_g|$ is the absolute band-gap energy. This relation is caused by the change in the hole effective mass (m_h) at the valence-band maximum (VBM). It is known that m_h at the VBM increases as the band-gap energy increases.[33] Furthermore the density of states (DOS) at VBM also increases as m_h increases.[33] The hybridization between the Mn 3*d* states and anion *p* bands is most important at VBM, because the lowest energy term of $3d^6\underline{L}$ states arises from the hybridization to the VBM of anion *p* bands. Square of V_{pd} involves a term that is proportional to the DOS at the VBM by comparing CI cluster model with impurity Anderson model;[34] thus, we can understand that the *p-d* exchange constant $N\beta$ increases as the band-gap energy increases. Therefore the *p-d* exchange constant $N\beta$ in narrow gap II-VI DMSs is weaker than that in wide gap II-VI DMSs.

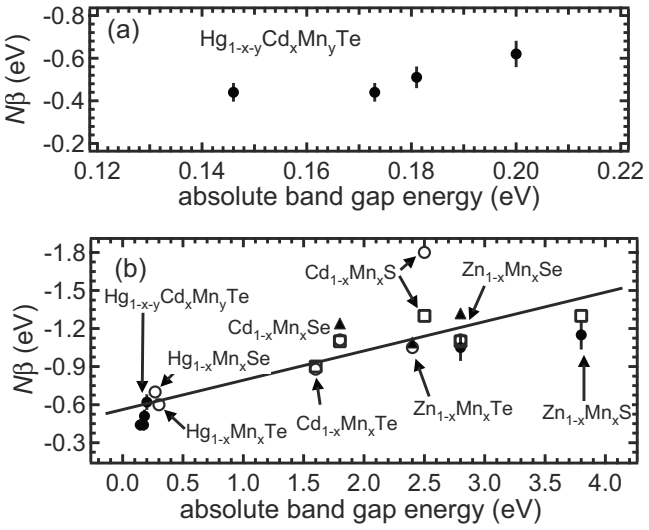

FIG. 7. (a) *p-d* exchange constant $N\beta$ for $Hg_{1-x-y}Cd_xMn_yTe$ with x=0–0.215 and $y\sim0.02$ as a function of the absolute band-gap energy. (b) Band-gap energy dependence of the *p-d* exchange constant $N\beta$ for various II-VI DMSs. Closed circles (this work), open circles (Ref. 2), triangles (Ref. 28), and squares (Refs. 7 and 8). The *p-d* exchange constant $N\beta$ versus band-gap energy at liquid He temperature for the Mn concentration nearly zero is plotted. The solid line corresponds to the least-squares fitting result.

As mentioned above, the *p-d* exchange constant $N\beta$ for $Hg_{1-x-y}Cd_xMn_yTe$ does not show the simple relation to the band-gap energy. This is caused by the different behaviors of heavy-hole mass (m_{hh}) and light-hole mass (m_{lh}) at VBM on the band-gap energy. In the negative to positive gap transition, the behavior of m_{hh} shows the linear dependence on the band-gap energy, while that of m_{lh} shows a linear depen-

dence on the absolute band-gap energy.[35] Therefore the DOS at VBM does not show the simple relation to the band-gap energy. Thus we can see that the behaviors of m_{hh} and m_{lh} around the negative to positive band-gap transition lead to the narrow spread of the *p-d* exchange constant $N\beta$ in $Hg_{1-x-y}Cd_xMn_yTe$.

IV. CONCLUSION

We have investigated the electronic structures and *p-d* exchange interaction of $Zn_{1-x}Mn_xY$ (Y=S,Se) and $Hg_{1-x-y}Cd_xMn_yTe$ by using the Mn 2*p* XPS, 2*p* XAS, 2*p*-3*d* RPES, and CI cluster model calculation. The reliable electronic structure parameters for $Zn_{1-x}Mn_xY$ (Y=S,Se) and $Hg_{1-x-y}Cd_xMn_yTe$ were obtained by the CI cluster model calculation that consistently reproduced both PES and XAS spectra by a single set of parameters. The obtained electronic structure parameters were compared with those for traditional II-VI DMS $Cd_{1-x}Mn_xTe$. We found that the strength of the *p-d* hybridization increases with increasing the band-gap energy of the host semiconductors. This behavior can be understood by the band-gap energy dependence of the DOS of anion *p* bands at the VBM. The evaluated *p-d* exchange constant $N\beta$'s for $Zn_{1-x}Mn_xY$ (Y=S,Se) and $Hg_{1-x-y}Cd_xMn_yTe$ were consistent with those of the previous work. In the Mn-doped wide and narrow gap II-VI DMSs, we found that the *p-d* exchange constant $N\beta$ is proportional to the absolute band-gap energy due to the change in the DOS of anion *p* bands, which hybridize with the Mn 3*d* orbitals, at the VBM. This result indicates that the *p-d* exchange interaction can be controlled by the band-gap energy in the DMSs.[27]

ACKNOWLEDGMENTS

The authors would like to thank A. Tanaka of Hiroshima University for allowing us to use the program for cluster model calculation and the staffs of SPring-8, especially T. Matsushita for developing software for XAS measurement. The RPES and XAS measurements were performed under the approval of Japan Synchrotron Radiation Research Institute (Proposals No. 1997B1043-NS-np and No. 1999A0404-U.S.-np). This work was partially supported by the Grant-in-Aid from the Ministry of Education, Culture, Sports, Science and Technology (MEXT), Japan.

*uedas@spring8.or.jp

[1] *Semimagnetic Semiconductors and Diluted Magnetic Semiconductors*, edited by M. Averous and M. Balkanski (Plenum, New York, 1991).
[2] J. K. Furdyna, J. Appl. Phys. **64**, R29 (1988) and references therein.
[3] M. Taniguchi, A. Fujimori, M. Fujisawa, T. Mori, I. Souma, and Y. Oka, Solid State Commun. **62**, 431 (1987).
[4] L. Ley, M. Taniguchi, J. Ghijsen, R. L. Johnson, and A. Fujimori, Phys. Rev. B **35**, 2839 (1987).
[5] R. Weidemann, H.-E. Gumlich, M. Kupsch, H.-U. Middelmann, and U. Becker, Phys. Rev. B **45**, 1172 (1992).
[6] M. Taniguchi, K. Soda, I. Souma, and Y. Oka, Phys. Rev. B **46**, 15789 (1992).
[7] T. Mizokawa and A. Fujimori, Phys. Rev. B **48**, 14150 (1993).
[8] T. Mizokawa and A. Fujimori, Phys. Rev. B **56**, 6669 (1997).
[9] S. Ueda, S. Suga, T. Iwasaki, A. Sekiyama, S. Imada, Y. Saitoh, and S. Takeyama, Jpn. J. Appl. Phys. **39**, Suppl. 39-1, 468 (2000).
[10] B. E. Larson and H. Ehrenreich, Phys. Rev. B **39**, 1747 (1989).
[11] H. Munekata, H. Ohno, S. von Molnar, A. Segmüller, L. L. Chang, and L. Esaki, Phys. Rev. Lett. **63**, 1849 (1989).
[12] H. Ohno, A. Shen, F. Matsukura, A. Oiwa, A. Endo, S. Katsumoto, and Y. Iye, Appl. Phys. Lett. **69**, 363 (1996).
[13] Y. Fukuma, H. Asada, M. Arifuku, and T. Koyanagi, Appl. Phys. Lett. **80**, 1013 (2002).
[14] M. Hashimoto, Y.-K. Zhou, M. Kanamura, and H. Asashi, Solid State Commun. **122**, 37 (2002).
[15] W. Giriat and J. K. Furdyna, in *Diluted Magnetic Semiconductors*, Semiconductors and Semimetals Vol. 25, edited by J. K. Furdyna and J. Kossut (Academic, New York, 1988), pp. 1–34.
[16] Y. Saitoh, T. Nakatani, T. Matsushita, T. Miyahara, M. Fujisawa, K. Soda, T. Muro, S. Ueda, H. Harada, A. Sekiyama, S. Imada, H. Daimon, and S. Suga, J. Synchrotron Radiat. **5**, 542 (1998).
[17] Y. Saitoh, H. Kimura, Y. Suzuki, T. Nakatani, T. Matsushita, T. Muro, T. Miyahara, M. Fujisawa, K. Soda, S. Ueda, H. Harada, M. Kotsugi, A. Sekiyama, and S. Suga, Rev. Sci. Instrum. **71**, 3254 (2000).
[18] S. Takeyama and S. Narita, Jpn. J. Appl. Phys., Part 1 **24**, 1270 (1985).
[19] T. M. Schuler, R. A. Stern, R. McNorton, S. D. Willoughby, J. M. MacLaren, D. L. Ederer, V. Perez-Dieste, F. J. Himpsel, S. A. Lopez-Rivera, and T. A. Callcott, Phys. Rev. B **72**, 045211 (2005).
[20] G. van der Laan and I. W. Kirkman, J. Phys.: Condens. Matter **4**, 4189 (1992).
[21] C. K. Shih, J. A. Silberman, A. K. Wahl, G. P. Carey, I. Lindau, W. E. Spicer, M. A. Berding, and A. Sher, J. Vac. Sci. Technol. A **5**, 3026 (1987).
[22] M. A. Berding, S. Krishnamurthy, A. Sher, and A.-B. Chen, J. Vac. Sci. Technol. A **5**, 3014 (1987).
[23] W. A. Harrison, *Electronic Structure and the Properties of Solids* (Freeman, San Fransisco, 1980).
[24] A. E. Bocquet, T. Mizokawa, T. Saitoh, H. Namatame, and A. Fujimori, Phys. Rev. B **46**, 3771 (1992).
[25] S. Takeyama, J. Kossut, and S. Narita, in *High Magnetic Fields in Semiconductor Physics*, edited by G. Landwehr (Springer-Verlag, London, 1987) Vol. 71, pp. 432–435.
[26] G. Bauer, J. Kossut, R. Faymonville, and R. Dornhaus, Phys. Rev. B **31**, 2040 (1985).
[27] J. A. Gaj, R. Planel, and G. Fishman, Solid State Commun. **29**, 435 (1979).
[28] D. R. Yoder-Short, U. Debska, and J. K. Furdyna, J. Appl. Phys. **58**, 4056 (1985).

[29] A. Balzarotti, M. Czyznyk, A. Kisiel, N. Motta, M. Podgorny, and M. Zimnal-Starnawska, Phys. Rev. B **30**, 2295 (1984).
[30] W.-F. Pong, R. A. Mayanovic, and B. A. Bunker, Physica B **158**, 617 (1989).
[31] W.-F. Pong, R. A. Mayanovic, B. A. Bunker, J. K. Furdyna, and U. Debska, Phys. Rev. B **41**, 8440 (1990).
[32] P. Kacman, Semicond. Sci. Technol. **16**, R25 (2001) and references therein.
[33] C. Kittel, *Introduction to Solid State Physics* (Wiley, New York, 1986).
[34] O. Gunnarson and K. Schonhammer, in *Handbook on the Physics and Chemistry of Rare Earths*, edited by K. A. Gschneider, L. Eyring, and S. Hufner (Elsevier, Amsterdam, 1987), Vol. 10, pp. 103–163.
[35] R. Dornhaus, G. Nimtz, and B. Schlicht, *Narrow Gap Semiconductors*, Springer Tracts in Modern Physics Vol. 98 (Springer-Verlag, Berlin, 1983).